7-11-2007

Scintillator counters with multi-pixel avalanche photodiode readout for the ND280 detector of the T2K experiment

O. Mineev
Institute for Nuclear Research of the Russian Academy of Sciences

A. Afanasjev
Institute for Nuclear Research of the Russian Academy of Sciences

G. Bondarenko
Center of Perspective Technologies and Apparatus (CPTA)

V. Golovin
Center of Perspective Technologies and Apparatus (CPTA)

E. Gushchin
Institute for Nuclear Research of the Russian Academy of Sciences

See next page for additional authors

Recommended Citation

Mineev, O., Afanasjev, A., Bondarenko, G., Golovin, V., Gushchin, E., Izmailov, A., Khabibullin, M., Khotjantsev, A., Kudenko, Y., Kurimoto, Y., Kutter, T., Lubsandorzhiev, B., Mayatski, V., Musienko, Y., Nakaya, T., Nobuhara, T., Shaibonov, B., Shaikhiev, A., Taguchi, M., Yershov, N., & Yokoyama, M. (2007). Scintillator counters with multi-pixel avalanche photodiode readout for the ND280 detector of the T2K experiment. *Nuclear Instruments and Methods in Physics Research, Section A: Accelerators, Spectrometers, Detectors and Associated Equipment, 577* (3), 540-551. https://doi.org/10.1016/j.nima.2007.04.161

Scintillator counters with multi-pixel avalanche photodiode readout for the ND280 detector of the T2K experiment

O. Mineev[a]*, A. Afanasjev[a], G. Bondarenko[b], V. Golovin[b], E. Gushchin[a], A. Izmailov[a], M. Khabibullin[a], A. Khotjantsev[a], Yu. Kudenko[a], Y. Kurimoto[c], T. Kutter[d], B. Lubsandorzhiev[a], V. Mayatski[e], Yu. Musienko[a], T. Nakaya[c], T. Nobuhara[c], B.A.J. Shaibonov[a], A. Shaikhiev[a], M. Taguchi[c], N. Yershov[a], M. Yokoyama[c]

[a] *Institute for Nuclear Research RAS, 117312 Moscow, Russia*
[b] *Center of Perspective Technology and Apparatus, 107076 Moscow, Russia*
[c] *Department of Physics, Kyoto University, Kyoto 606-8502, Japan*
[d] *Department of Physics and Astronomy, Louisiana State University Baton Rouge, Louisiana 70803-4001, USA*
[e] *AO Uniplast, 600016 Vladimir, Russia*

Abstract

The Tokai–to–Kamioka (T2K) experiment is a second generation long baseline neutrino oscillation experiment which aims at a sensitive search for the ν_e appearance. The main design features of the T2K near neutrino detectors located at 280 m from the target are presented. Scintillator counters developed for the T2K near detectors are described. Readout of the counters is provided via WLS fibers embedded into S–shape grooves in a scintillator and viewed from both ends by multi–pixel avalanche photodiodes operating in a limited Geiger mode. A description, operational principles and the results of tests of photosensors with a sensitive area of 1.1 mm^2 are presented. A time resolution of 1.5 ns, a spatial resolution of 9.9–12.4 cm, and a MIP detection efficiency of more than 99% were obtained for scintillator detectors in a beam test.

*Corresponding author. *Email address:* oleg@inr.ru

1 Introduction

The T2K project [1] is a second generation long baseline neutrino oscillation experiment which will use a high intensity off–axis neutrino beam produced by the JPARC 50 GeV (initially 40 GeV) proton beam. The first phase of the T2K experiment pursues two main goals: a sensitive measurement of θ_{13} and a more accurate determination of the parameters $\sin^2 2\theta_{23}$ and Δm^2_{23} than any previous experiment.

To achieve the physics goals, it is important to provide precise measurements of the neutrino beam properties, neutrino flux, spectrum and interaction cross sections. For these purposes, the near detector complex (ND280 [2]) will be built at the distance of 280 m from the target along the line between the average pion decay point and the Super-Kamiokande detector. In order to keep the systematics uncertainties below the statistical error, the physics requirements for ND280, discussed in detail in Ref. [2], can be briefly summarized as follows. The energy scale of the neutrino spectrum must be understood at the 2% level, and the neutrino flux should be monitored with better than 5% accuracy. The momentum resolution of muons from the charged current quasi–elastic interactions should be less than 10%, and the threshold for the detection of the recoil protons is required to be about 200 MeV/c. The ν_e fraction is to be measured with an uncertainty of better than 10%. The measurement of the neutrino beam direction with precision much better than 1 mrad is expected to be provided by the on–axis detector (neutrino monitor). The off–axis ND280 is shown in Fig. 1 and consists of the UA1 magnet operated with

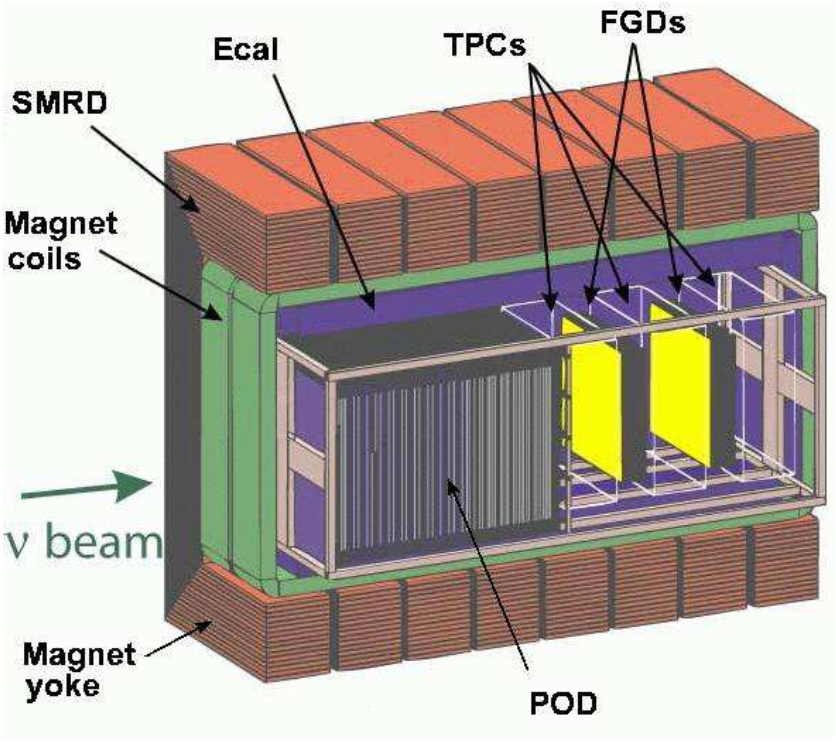

Figure 1: The cutaway view of the T2K near detector.

a magnetic field of 0.2 T, a Pi-Zero detector (POD), a tracking detector which includes time projection chambers (TPC's) and fine grained scintillator detectors (FGD's), an electromagnetic calorimeter (Ecal), and a side muon range detector (SMRD).

The POD has been designed to be similar to the MINERνA detector [3]. It is installed in the upstream end of the magnet and optimized for measurement of the inclusive π^0 production by ν_μ on oxygen. The POD consists of 76 tracking planes composed of triangular polystyrene scintillating bars (about 2×10^4) alternating with thin (0.6 mm) lead foils. Each bar has a 3 cm base, 1.5 cm height and a central hole for a WLS fiber. Three TPC's will measure the 3–momenta of muons produced by charged current interactions in the detector and will provide the most accurate measurements of the neutrino energy spectrum. The ND280 will contain two FGD's, each with dimensions $2 \times 2 \times 0.3$ m^3 resulting in a total target mass of 1.2 tons. The first FGD will be an active scintillator detector, similar to the SciBar [4] detector of the K2K experiment [5]. Each FGD layer will consist of 200 scintillator bars, and thirty layers will be arranged in alternating vertical and horizontal layers perpendicular to the beam direction. The second FGD will consists of $x - y$ layers scintillator bars alternating with 3 cm thick layers of passive water. The Ecal surrounds the POD and tracking region and consists of 15 layers, each of which has one sheet of 3 mm Pb alloy and one layer of 1 cm thick $\times$ 5 cm wide plastic scintillator bars (with signal readout by WLS fibers). Interior to this section is the preradiator section, where each of the 3 layers consists of a lead alloy sheet backed by 3 layers of scintillator bars. Air gaps in the UA1 magnet will be instrumented with plastic scintillator to measure the ranges of muons which escape at large angles with respect to the neutrino beam and which can not be measured by the TPC's. The active component of the SMRD will use scintillators with wavelength shifting fibers (WLS) readout to transport the light into photosensors.

The ND280 detector will widely use WLS fiber readout with light detection from fibers by photosensors which have to operate in a magnetic field environment and limited space inside the UA1 magnet. The primary candidate for the photosensor is the multi–pixel avalanche photo-diode operating in the limited Geiger multiplication mode [6,8–10]. Such photodiodes are compact, well matched to spectral emission of WLS fibers, and insensitive to magnetic fields [11, 12].

2 Geiger mode multi–pixel avalanche photodiodes

2.1 Overview

The multi-pixel avalanche photodiodes with a metal–resistor–semiconductor layer structure operating in the limited Geiger mode (hereafter referred to as MRS APD's or MRS photodiodes) are invented and designed by the Center of Perspective Technologies and Apparatus (CPTA), Moscow [6]. Detailed description of these devices and principles of operation can be found in Refs. [7, 9, 13]. Such a photosensor consists of many pixels on a common p–type silicon substrate. A simplified topology of a MRS photodiode is shown in Fig. 2. Each pixel operates as an independent Geiger micro-counter with a gain of the same order as a vacuum photomultiplier. Geiger discharge is initiated by a photoelectron

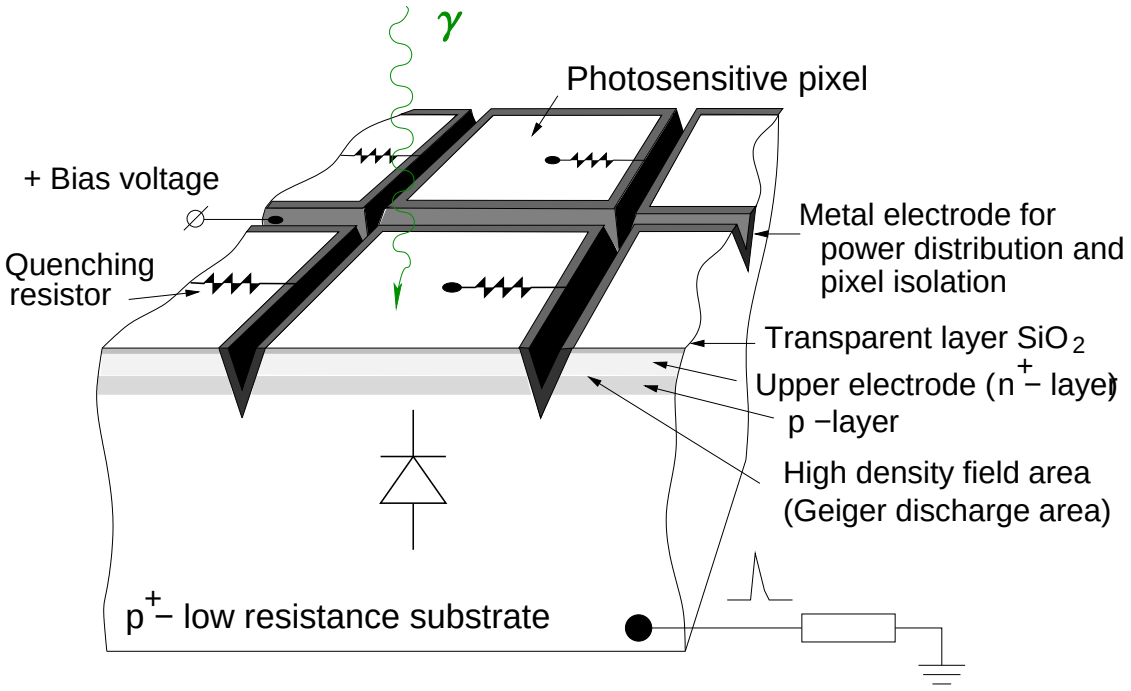

Figure 2: The schematic view of the MRS photodiode structure.

in the high electric field created in a very thin layer of about 1 μm by the applied bias voltage. The discharge current for each pixel produces a voltage drop at individual resistors. As a result, the electric field density becomes small and can no longer support the discharge quenched in such a way. Small pixels are separated by grooves filled with an optically non–transparent material to suppress the cross–talks. The gain is determined by the charge accumulated in a pixel capacitance: $Q_{pixel} = C_{pixel} \cdot \Delta V$, where ΔV is difference between the bias voltage and the breakdown voltage of the diode (overvoltage). Since ΔV is about a few volts and $C_{pixel} \simeq 50$ fF, then typical $Q_{pixel} \simeq 150$ fC, that corresponds to 10^6 electrons. A single incident photon can fire more than one pixel. Thus, the gain of the MRS photodiode is equal to the charge of a pixel multiplied by the average number of pixels fired by a single photon.

The amplitude of a single pixel signal does not depend on the triggered number of carriers in this pixel. In such a way, the photodiode signal is a sum of fired pixels. Each pixel operates as a binary device, but the multi–pixel photodiode as a whole unit is an analogue detector with a dynamic range limited by the finite number of pixels. The pixel size can be 15×15 to 70×70 μm^2, and the total number of pixels is 100–4000 per mm^2. We tested the CPTA MRS photodiodes with a sensitive area of 1.1 mm^2 with 556 pixels of 45×45 μm^2 size (see Fig. 3).

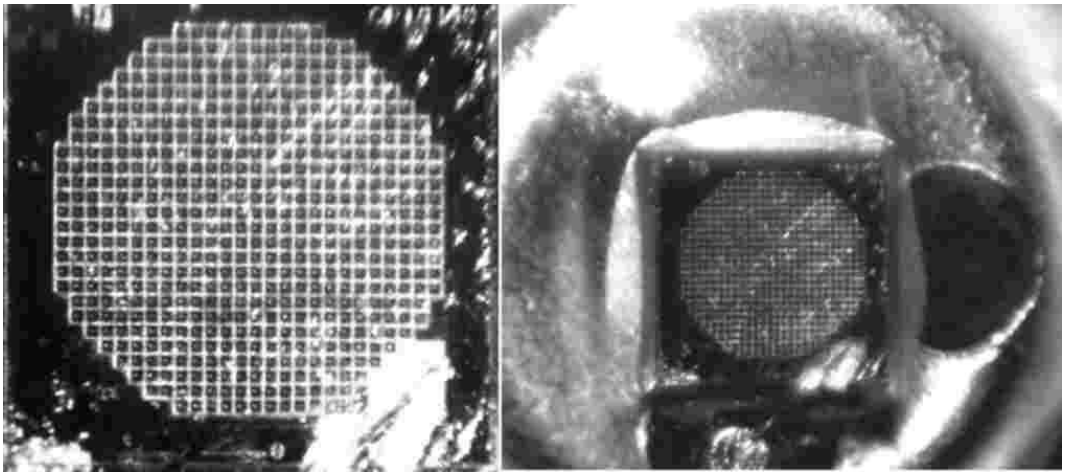

Figure 3: Face view of a MRS avalanche photodiode with 556 pixels, magnified 56 times (left) and 14 times (right). The sensitive area has an octagonal shape with an 1.2 mm side–to–side distance.

2.2 Basic properties of the CPTA MRS photodiodes

The main parameters of the MRS photodiodes such as the gain, photon detection efficiency, intrinsic noise, cross–talk, depend on the applied bias voltage. The MRS photodiodes were tested using a signal from a green light emitting diode (LED). The MRS signal was amplified and split into two signals: one was fed to a discriminator, another was measured by an ADC with a gate of about 100 ns.

Gain. A typical operating voltage is around 40 V for the tested MRS photodiodes, although the voltage can differ by a few volts to provide the same gain in photodiodes. The MRS photodiode has an excellent single photoelectron (p.e.) resolution determined mainly by electronics noise even at room temperature. It means that there is only a small pixel to pixel gain variation as well as small fluctuations in Geiger discharge development. The absolute gain depends on the photodiode topology, bias voltage and temperature. The voltage and temperature sensitivities of the MRS photodiode gain are rather weak as will be demonstrated below. A 0.1 V change in bias voltage corresponds to a 2–3% variation in gain. The charge of a single p.e. signal in a calibrated ADC was used to determine the MRS photodiode gain. The typical gain value at room temperature (22°C) is obtained to be about 0.5×10^6.

Photon detection efficiency. The photon detection efficiency (PDE) of a multi-pixel avalanche photodiode operating in the limited Geiger mode is a product of 3 factors:

$$\mathrm{PDE} = QE \cdot \varepsilon_{Geiger} \cdot \varepsilon_{pixel}, \tag{1}$$

where QE is the wavelength dependent quantum efficiency, ε_{Geiger} is the probability for a photoelectron to initiate the Geiger discharge, ε_{pixel} is a fraction of the total photodiode area occupied by sensitive pixels. The bias voltage affects one parameter in expression (1) ε_{Geiger}. The geometrical factor ε_{pixel} is completely determined by the MRS photodiode

topology. Its value is estimated to be about 70–80% in an ideal case. The absolute value of the PDE was measured using small pulses from a green LED (525 nm) which illuminated a MRS photodiode through a 0.5 mm diameter collimator. The number of emitted photons was obtained using a calibrated PMT XP2020. The normalized PDE values at 525 nm for different bias voltages are presented in Fig. 4. The cross-talk contribution was subtracted

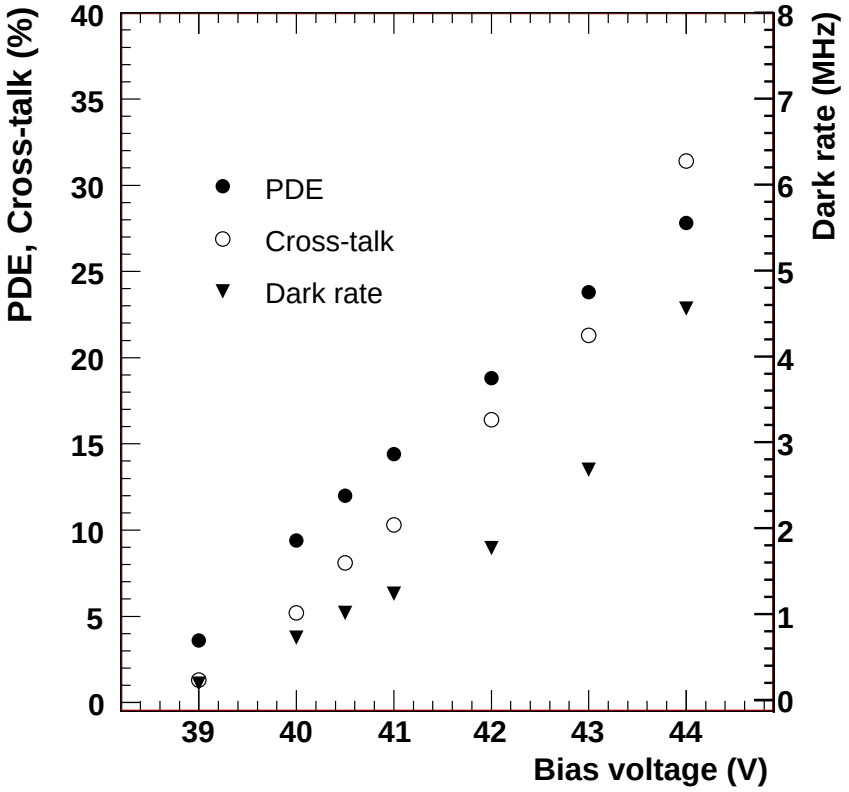

Figure 4: The photon detection efficiency, cross–talk and dark rate as a function of the applied bias voltage.

from the signal to obtain the correct value of the PDE, the accuracy of which is estimated to be about 20%. As seen in Fig. 4, the PDE is about 12% at a dark rate of 1 MHz. The PDE can be increased up to almost 30% at the expense of much higher dark rate.

The PDE dependence on the wavelength of the detected light, as well as the emission spectrum of the WLS fiber Y11 are shown in Fig. 5. The peak emission of the fiber depends on its length due to the absorption of the light. The spectral response of a MRS photodiode was measured in a spectrophotometer calibrated with a PIN–diode [15]. The PDE was measured at higher V_{bias} and, therefore, the dark rate was higher (about 2.3 MHz for a discriminator threshold of 0.5 p.e.). The PDE decreases by about 50% when V_{bias} is lowered such that the dark rate is ~ 1 MHz.

Dark rate. The limiting factor for a wide application of the MRS photodiodes in the

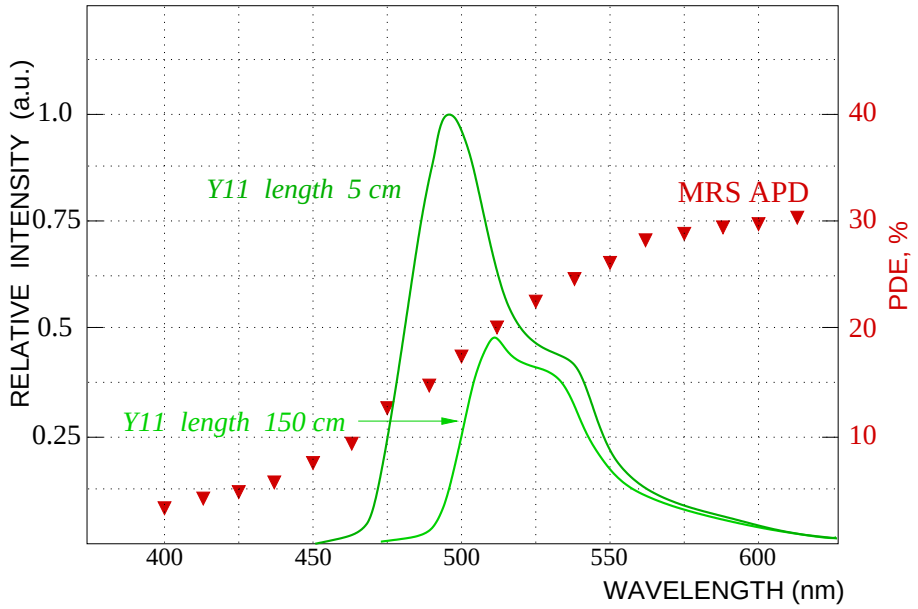

Figure 5: Light emission spectrum of the Y11(150) fiber (from Kuraray plots [14]) and the PDE of a MRS photodiode.

readout of scintillators is the dark noise rate which originates from thermally created carriers in the depletion region under high electric fields. The dark rate mainly consists of single p.e. pulses. Larger amplitude pulses also contribute to the dark rate, as shown in Fig. 6. However, the intensity of the pulses with 2 p.e. amplitudes is about 15 times less than the intensity of the single p.e. pulses. Large amplitudes (> 1 p.e.) are generated by the optical cross-talk as well as by accidental pile-ups between the independent pixels, though the second effect is relatively small. The dark rate decreases to the level of a few kHz for the threshold of 2.5 p.e. The intensity of 1 p.e. pulses as well as 2 p.e. pulses is significantly higher for higher bias voltage, as can be seen from Fig. 6 in case of $V_{bias} = 39.8$ V. Dark pulses and mostly leakages create the dark current through a MRS photodiode in a typical range of $0.3 - 1.0\ \mu A$. The dark rate decreases to about 1 kHz/mm^2 at -70°C, i.e. decreases by a factor of 2 for every temperature drop of $9-10$°C for a threshold of 0.5 p.e. and and the condition of keeping the gain at a constant value by tuning the bias voltage.

Optical cross–talk. A single incident photon can create more than a single p.e. due to optical cross–talk. The mechanism of this effect is not quite clear. Models predict that during the Geiger discharge and recombination of carriers infrared photons are emitted. These photons penetrate into the adjacent pixels and fire them. Optical cross–talk leads to a higher than expected signal as Geiger discharge occur in additional pixels. The absolute value of the cross–talk can be calculated by assuming a Poisson distribution for the number of photoelectrons observed in response to the light from a LED. When the MRS photodiode noise is small, the measured mean number of fired pixels by the LED

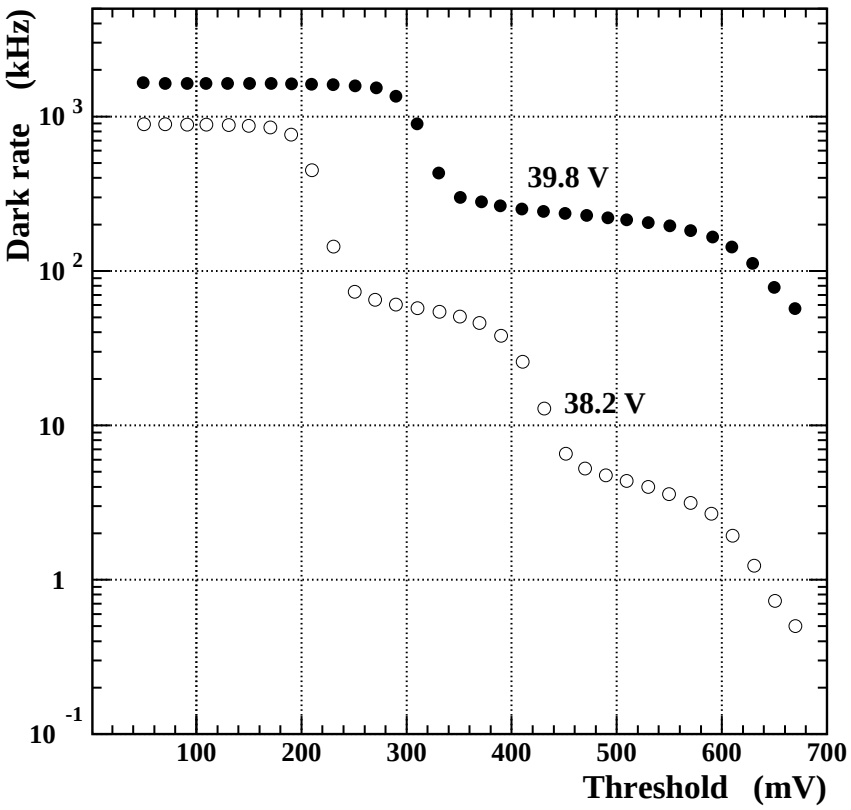

Figure 6: Dark rate vs the discriminator threshold for two bias voltages. The discriminator threshold values of 100, 300, and 500 mV correspond to 0.5 p.e., 1.5 p.e., and 2.5 p.e., respectively, for $V_{bias} = 38.2$ V.

photons, $\bar{N}_{LED}$, is compared with the calculated value $\bar{N}_{pe}$ given by

$$\bar{N}_{pe} = -lnP(0), \tag{2}$$

where $P(0)$ is the fraction of 0 p.e., or "pedestal" events. Then the deviation of the ratio $\bar{N}_{LED}/\bar{N}_{pe}$ from 1 gives the cross–talk value. These values are presented for several bias voltages in Fig. 4. A cross–talk value of about 5% was obtained at a bias voltage that provides a dark noise rate of ≤ 1 MHz at a discriminator threshold of 0.5 p.e. The cross–talk is larger for higher bias voltage. The sharp decrease of the dark rate shown in Fig. 6 is a good demonstration of the low optical cross–talk. It should be noted that the signal amplitude in photoelectrons is less than the measured amplitude determined as the average number of fired pixels by the cross-talk value, i.e. by a few per cent.

Temperature dependence. The PDE and gain of MRS photodiodes (as well as the signal amplitude) are expected to be sensitive to temperature because the breakdown voltage depends on temperature. The MRS signal amplitude (light yield) is proportional

to $N_{\rm photons} \times$ PDE $\times$ gain, where $N_{\rm photons}$ is the number of photons from the LED which illuminate the photodiode. The parameters of the MRS photodiodes were measured over temperatures from 15° to 33°C. The temperature variation of the MRS signal (a green LED was used as a light source) is presented in Fig. 7. The MRS signal dependency

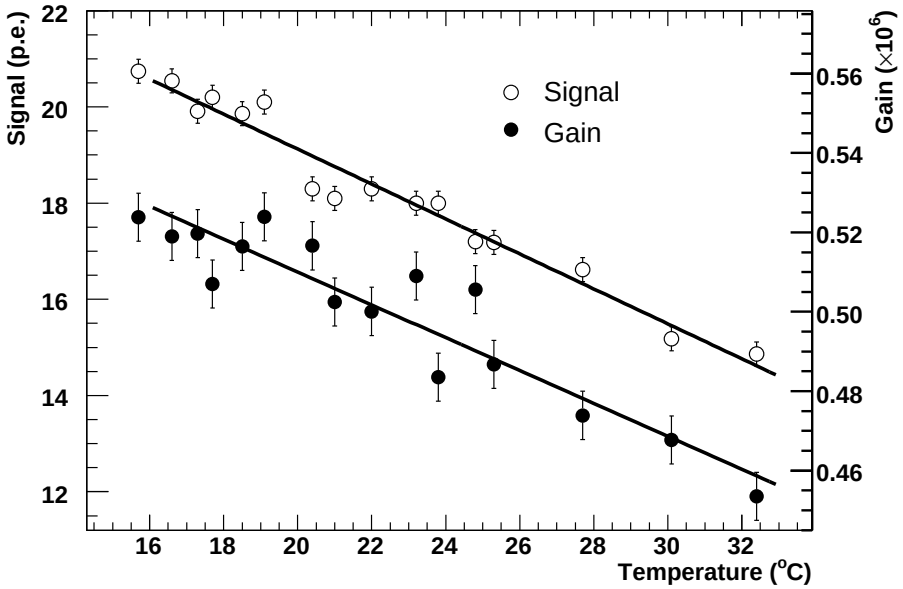

Figure 7: The MRS signal from a green LED and gain as a function of the ambient air temperature.

of -1.5 %/°C is obtained for increasing temperature. The MRS gain itself decreases with temperature as -1.2 %/°C (see Fig. 7), while the PDE varies with temperature as -0.3 %/°C. The dark rate depends on temperature with a coefficient of 62 kHz/°C, as shown in Fig. 8. Decreasing the temperature below 0°C greatly reduces the noise and increases the PDE, as shown in Ref. [15].

Recovery time. The ability of MRS photodiodes to operate at high counting rates was tested using two LED signals. We measured the amplitude of the second signal $A_2(t)$ as a function of the time difference t between the first and second signal. Fig. 9 shows the ratio $A_2(t)/A_2(0)$, where $A_2(0)$ is the amplitude of the second signal when the first LED signal is off. As seen from Figure 9, a minimum time interval between the first and second pulse of about 5 μs is needed to recover about 95% of the full amplitude of the second signal. This long recovery time is due to the fact that the individual resistor of each pixel, R_{pixel}, has the value of about 20 MΩ, the pixel capacitance C_{pixel} is typically 50 fF that gives $\tau = R_{pixel} \cdot C_{pixel} \sim 1\mu$s.

Dynamic range and linearity. The dynamic range of the MRS photodiode is limited by the finite number of pixels. The saturation of the MRS photodiode in response to large light signals is shown in Fig. 10. In this test, the LED signal was ajusted to obtain similar response for both PMT and MRS photodiode at the light yield below 150 p.e. The

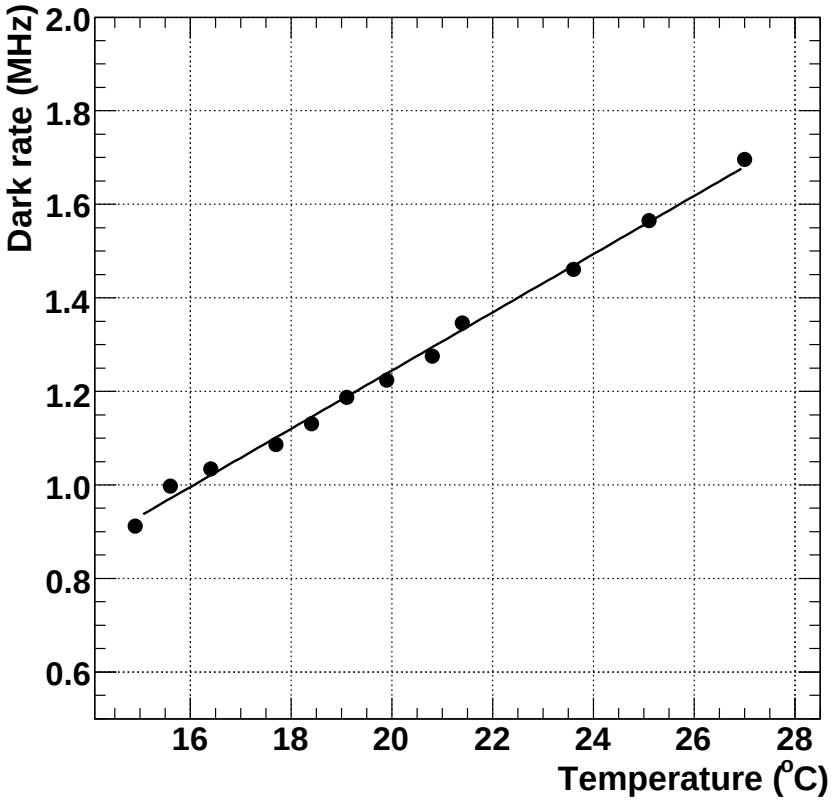

Figure 8: The dark rate for threshold of 0.5 p.e. vs the ambient air temperature.

photodiode signal is linear for low amplitutes. A nonlinearity of about 10% is already seen for a signal of 150–200 p.e. For the PMT signal of 500 p.e., the MRS photodiode has a 30% smaller signal than that of the PMT. Full saturation of the 556 pixel MRS photodiode starts at a reference (PMT) signal of more than 2000 p.e.

Timing. The development of the Geiger discharge in a small depth ($\sim 0.8\ \mu m$) of the depletion region takes a few hundred picoseconds. The typical rise time is 1 ns, the decay time is determined by the pixel capacitance. A laser with a wavelength of 635 nm and a pulse width of 35 ps (fwhm) was used to measure the intrinsic time resolution of 1 p.e. pulses. Very weak laser light created only 1 p.e. signals in a MRS photodiode. The time resolution obtained for a threshold of 0.2 p.e. at 22°C is presented in Fig. 11.

Life time. The failure rate of the MRS photodiodes is an important figure of merit for the overall detector performance, because most photodiodes can not be replaced without significant disassembly of the ND280 detector. Exposures to elevated temperature are used to evaluate the expected life time of semiconductor devices. We have placed 19 MRS photodiodes in an oven at 80°C for 30 days. All photodiodes were kept under bias voltages to provide the same dark current as at room temperature. One of the devices started to conduct a large current after a week of heating. The failed device had the

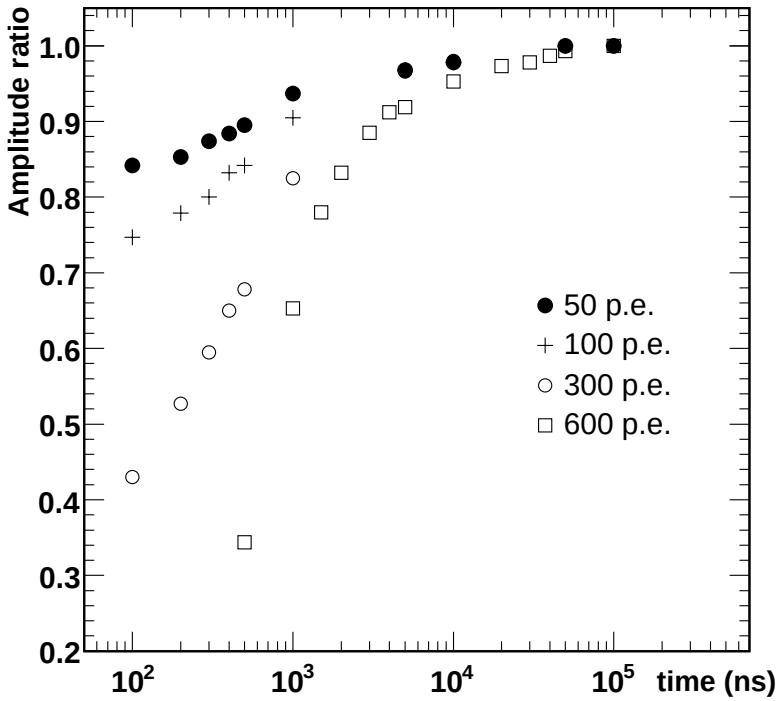

Figure 9: The relative amplitude of the MRS delayed signal from a LED as a function of the time difference between the first LED pulse and the second one. The amplitude is normalized to its value when the first LED signal is off. The amplitudes of the first signal are 50, 100, 300, 600 photoelectrons.

worst PDE among of the tested devices. This points to a possible defect in its structure. All other devices passed the test without residual effects, and the LED signals measured by these MRS diodes after a period of 30 days of elevated temperatures did not show any significant degradation. The signals of the tested photodiodes in response to a LED photons were measured before the heating and for a period of about 260 days after the heating. The results for two devices are presented in Fig. 12. The accuracy of the l.y. measurements is about 2.0 p.e. (rms) due to misalignments between the fiber and the MRS photodiodes that are estimated to be between 20 and 100 μm in this series of tests. For more than 7 months after heating no degradation in the light yield was observed.

Two hundred MRS photodiodes fabricated from a few different wafers were tested. In order to meet the requirements of the experiment, the dark rate of each device should be kept close to a reference value of 1 MHz at room temperature 22°C and for a discriminator threshold of 0.5 p.e. This required the individual adjustment of the bias voltage of 38 to 42.1 V for each photodiode, that in turn resulted in a wide range of 8.9–18.8% for the PDE values, and the gains of these 200 MRS photodiodes were found to be between 0.34×10^6 and 0.69×10^6.

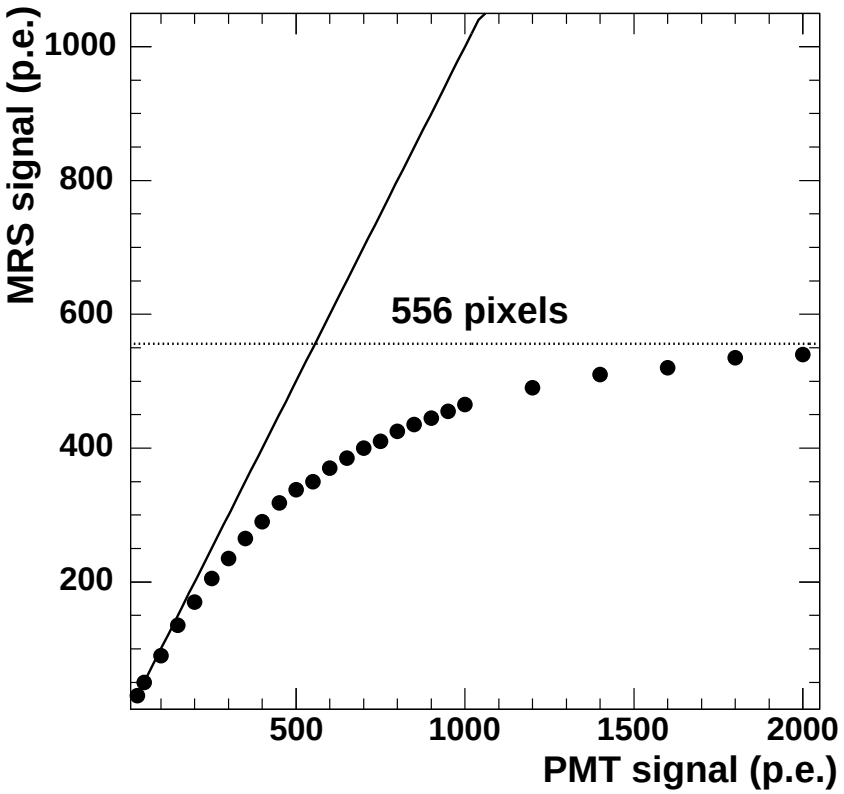

Figure 10: The MRS photodiode response vs the PMT signal. The signal of the MRS photodiode is saturated at the level of the maximum number of 556 pixels.

3 Scintillator detectors with WLS fiber readout

Several subdetectors of the T2K near detector complex will be composed of many scintillator detectors: rectangular and triangular scintillator bars, and various scintillating slabs. All these elements use embedded WLS fibers to read light from the scintillators. A well known design will be adopted for the bars with WLS fibers: one straight hole or groove on one surface for a WLS fiber. For large scintillator slabs (SMRD, active elements of Ecal), the usage of the standard readout scheme with several equidistant WLS fibers which run along the slab is not appropriate due to mechanical constraints of the UA1 magnet. We consider extruded scintillator slabs with a double–ended WLS fiber readout technique as active elements for the SMRD detector. Instead of a few parallel WLS fibers we propose to use a single long WLS fiber embedded in an S–shape groove which reduces the maximum path length that light has to travel within the scintillator to a few cm. The detector prototypes were manufactured using an extrusion technique developed at the Uniplast Factory, Vladimir, Russia. The scintillator is etched by a chemical agent that results in the formation of a micropore deposit over the plastic surface. The thick-

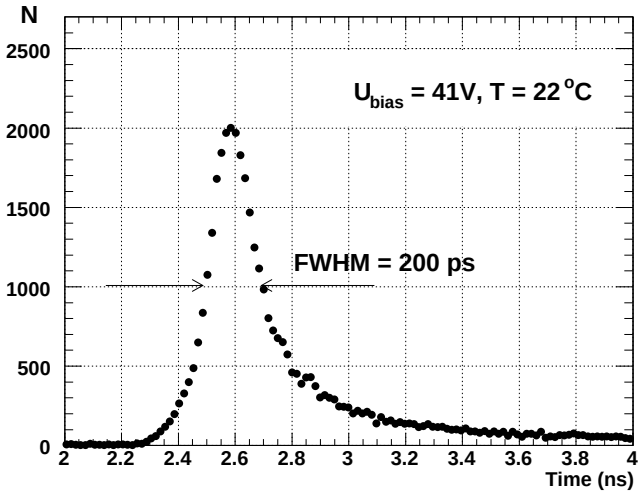

Figure 11: Time spectrum of single photoelectron signals obtained by a MRS photodiode at 22°C.

ness of the deposit (30–100 μm) depends on the etching time. Details can be found in Ref. [16]. A scintillator slab of 1x17x87 cm^3 with an S–shaped groove of 3 mm depth was manufactured for a test in a pion/proton beam. The half–period of the S–shape groove is 58 mm, as shown in Fig. 13. A 2.55 m long multi–clad Kuraray Y11 (200 ppm dopant) WLS fiber of 1 mm diameter is embedded into the groove with an optical grease and both ends are attached to MRS photodiodes. To avoid the degradation of the Y11 parameters in real SMRD counters, the bending procedure to make 3 cm radius loops will be done at the temperature of about 80°C.

This module was first tested with cosmic muons. A light yield (l.y.) of 16.4 p.e. was obtained for MIP's in the center for summed signals from both photodiodes. In order to suppress the timing spread caused by the trigger counters the combination $(TDC_{left} - TDC_{right})/2$ was used to measure the time resolution. A time resolution of $\sigma = 1.57$ ns was obtained for MIP's which passed through the central part of the slab.

4 Beam tests of the SMRD prototype

4.1 Beam test setup

A beam test of extruded scintillators with embedded WLS fibers was performed at the KEK 12-GeV proton synchrotron with 1.4 GeV/c protons and pions. Two counters were placed in a beam and tested simultaneously. One was the S–grooved scintillator (S–counter) described in the previous section, another one was a scintillator slab, 1x18x50 cm^3 in size, with a single straight groove in the middle of the plastic (W–counter). An 1.11 m long Kuraray Y11(200) fiber of 1 mm diameter was embedded with optical grease into

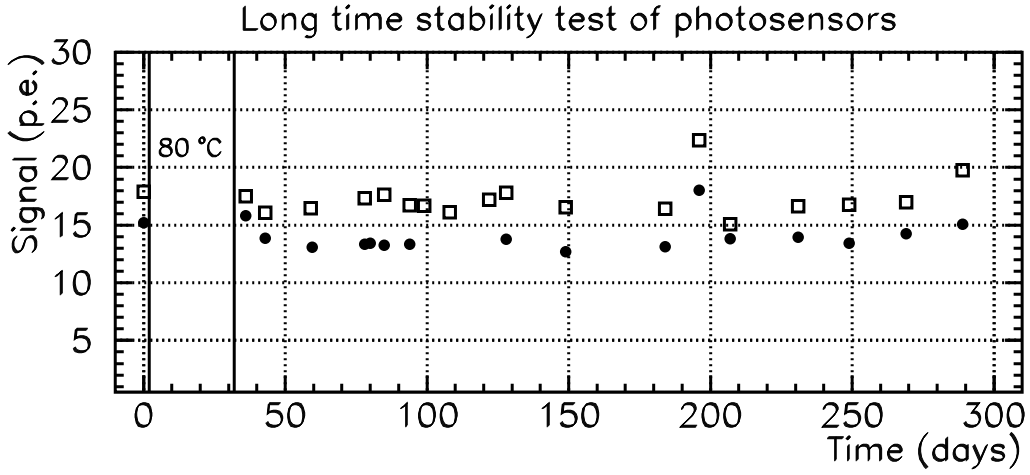

Figure 12: Light yields of two MRS photodiodes measured with a green LED before and after the heating test. The heat exposure at 80°C lasted for 30 days. Successively, the photodiodes were monitored for 260 days. The signals were corrected for temperature changes in the range from $18 - 27$°C. Each point has an error of ± 2.0 p.e.

the straight groove of the W–counter. The fiber in each counter is viewed from both ends by MRS photodiodes. The fibers are directly coupled to photosensors inside special sockets. The detectors were mounted on a platform which could be moved horizontally and vertically with respect to the beam line. Upstream of the counters, a TOF system was used to separate pions and protons. Finger trigger counters restricted the beam spot size to a $10 \times 10\text{mm}^2$ square. The signals were amplified by fast hybrid preamps mounted directly behind the photodiodes. The bias voltage was set individually for each MRS photodiode to limit the dark rate to about 1.2 MHz for a 0.5 p.e. threshold. A simplified electronic diagram of the beam test setup is shown in Fig. 14.

Only pions were selected for analysis as their response is close to that expected from MIP's in the T2K experiment. The ambient temperature drifted between 15–18°C during the beam test. Typical ADC spectra from pions are shown in Fig. 15. In this Figure, one spectrum is obtained with a bias voltage of 38.7 V which corresponds to a dark rate of 0.86 MHz for a discriminator threshold of 0.5 p.e. The second spectrum is measured with a bias voltage of 40.9 V corresponding to a dark rate of almost 2 MHz. The individual photoelectron peaks are clearly separated at 38.7 V and still visible at 40.9 V.

4.2 Detection efficiency of MIP's

The light yield scan over the S–counter surface is presented in Table 1. The beam spot spreads beyond the scintillator area near the edges at $y = \pm 80$ mm causing the small l.y. values. If the edges are ignored, the light output over the S–counter (sum of both

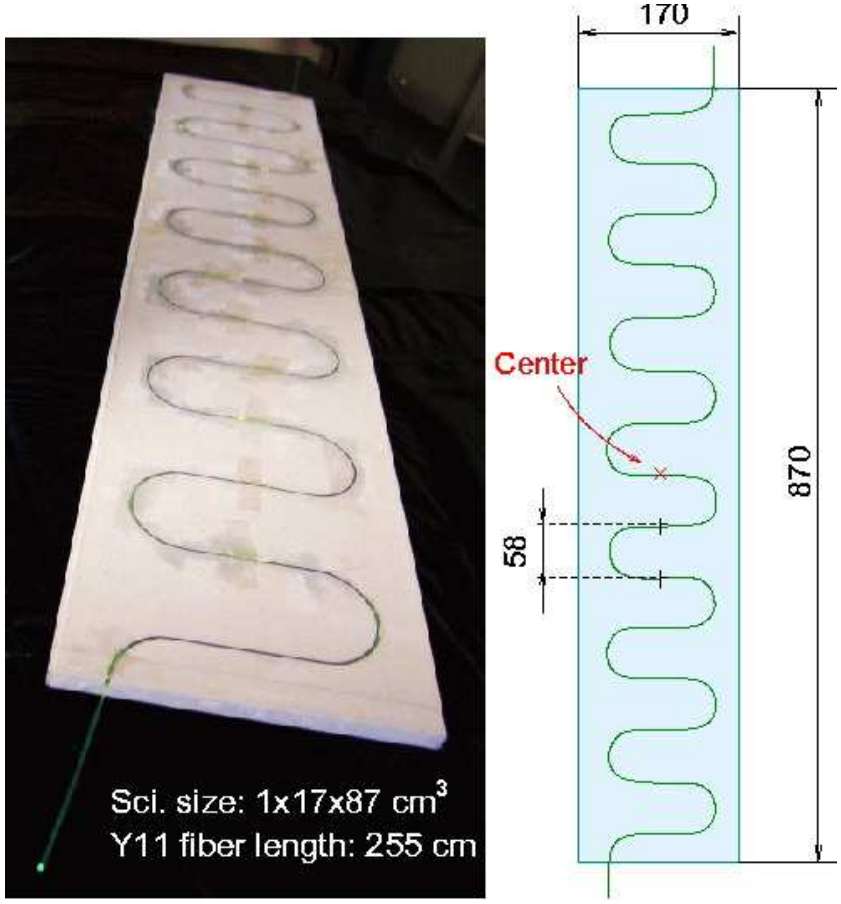

Figure 13: Scintillator slab with S–shaped fiber readout: photograph (left) and schematic view (right).

end signals) varies from 12 to 20 p.e./MIP. The largest l.y. is measured at the ends, close to either of the two MRS photodiodes. In order to obtain the detection efficiency the ADC spectra were analyzed. The event is considered accepted if its ADC amplitude exceeds a certain threshold set in number of p.e. The average statistics in each location is about 2000 events. Table 2 demonstrates the S–counter pion detection efficiency when the threshold for the sum of both end signals is set to 2.5 p.e. The detection efficiency is close to 100 % except for the edge area where a part of the beam missed the counter due to some misalignment between the beam counters and the tested detector. For a higher threshold of 4.5 p.e set for the sum of the amplitudes from the two ends, the MIP detection efficiency is greater than 98%. We can conclude that the l.y. of more than 12 p.e. (sum of both ends) satisfies the requirement for the S–counter to provide a detection efficiency greater than 99% for a MIP. If we require that each MRS photodiode signal exceeds 0.5 p.e. the MIP detection efficiency is found to be about 99.5%.

To make a detailed scan along the middle line of the S–counter the size of the beam spot was reduced to 0.5×0.5 cm^2. The result is shown in Fig. 16. The WLS fiber route

Table 1: Light yield (p.e./MIP) over the S–counter. Sum of the signals from both ends. The bias voltage of 38.7 V was applied to both MRS photodiodes.

y, mm x, mm	-80	-60	-40	-20	0	20	40	60	80
-406	6.3	11.9	13.2	16.0	17.8	18.6	18.7	18.8	13.8
-319	10.2	11.6	14.7	15.7	15.9	16.4	17.3	16.7	13.2
-200	10.2	12.7	14.3	16.0	15.5	16.6	18.2	18.7	15.0
-87	10.4	11.7	13.0	15.0	15.0	15.4	16.3	14.5	11.0
-30	8.8	14.4	16.4	16.2	15.3	14.6	13.8	12.9	10.9
0	11.0	12.9	14.8	14.3	15.3	16.2	14.9	13.9	11.7
30	9.3	11.8	12.6	14.4	14.8	15.8	16.8	16.0	13.0
87	12.3	14.4	15.1	14.6	14.2	14.7	14.2	12.9	11.8
200	11.0	15.2	16.0	15.9	15.6	15.5	13.7	12.9	11.3
319	12.6	16.1	17.4	16.3	15.5	15.2	14.5	12.3	10.4
406	11.8	12.9	17.9	19.9	20.0	19.1	19.1	16.2	11.9

Table 2: Detection efficiency over the S–counter for a threshold of 2.5 p.e. The bias voltage of 38.7 V was applied to both MRS photodiodes.

y, mm x, mm	-80	-60	-40	-20	0	20	40	60	80
-406	0.660	0.995	0.999	1.000	1.000	0.999	1.000	1.000	0.999
-319	0.750	0.999	0.999	0.999	0.999	0.999	0.999	0.998	1.000
-200	0.788	0.998	0.999	0.999	1.000	1.000	0.999	0.999	1.000
-87	0.839	0.996	0.998	0.999	1.000	0.999	1.000	0.999	0.995
-30	0.886	0.999	0.999	1.000	1.000	0.999	1.000	0.997	0.998
0	0.985	0.998	0.997	0.998	0.996	0.998	0.999	0.999	0.998
30	0.918	0.996	0.998	0.999	1.000	1.000	1.000	0.999	0.998
87	0.989	0.997	1.000	0.999	0.999	1.000	0.998	0.999	0.996
200	0.995	0.998	1.000	0.999	1.000	1.000	1.000	0.999	0.994
319	0.999	0.998	1.000	1.000	1.000	1.000	1.000	0.998	0.994
406	0.998	0.999	1.000	1.000	1.000	0.999	1.000	1.000	0.984

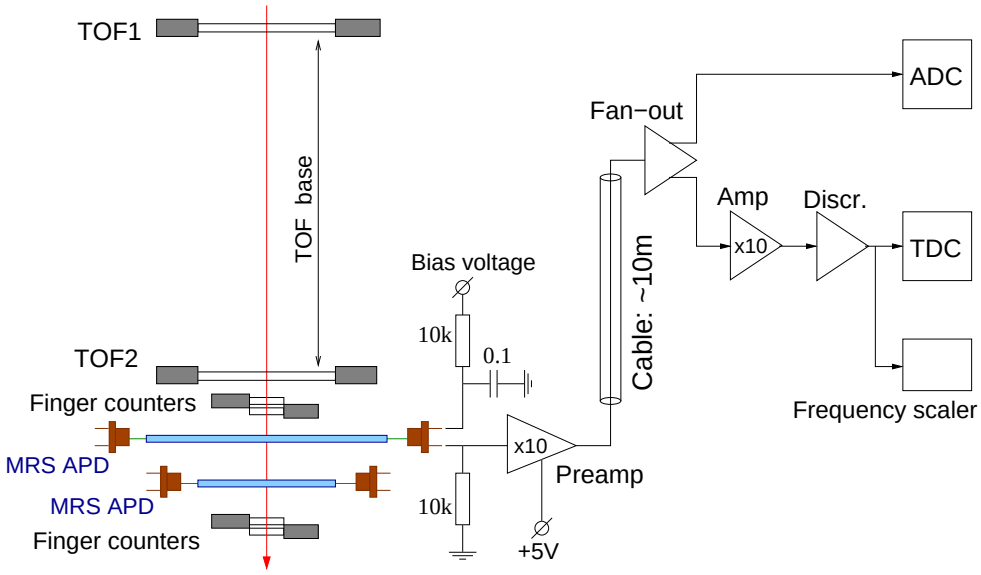

Figure 14: The electronic readout diagram used in the beam test.

is clearly reflected in the pattern of the l.y. distribution along the x–axis. A maximum l.y. is observed in points where the beam crosses the fiber, while the l.y. drops by about 20% in between the fiber segments. Fig. 17 shows the result of the transverse l.y. scan across the W–counter, which has a single straight groove running down the middle of the counter. The attenuation length of scintillation light before capture by the WLS fiber is obtained to be 9.0 ± 1.3 cm and 7.2 ± 1.2 cm for the upper and the lower part of the W–counter, respectively. These values are consistent within measurement uncertainty, and the average attenuation length of such a counter is estimated to be about 8.1 ± 0.9 cm.

4.3 Time and spatial resolution of the S–counter

The time resolution was measured with the discriminator thresholds set to a level of 0.5 p.e. for each MRS photodiode. To suppress the timing spread caused by the trigger counters (as in the cosmic ray test) we used the combination $(T_{left} - T_{right})/2$ to determine the time resolution. The dependence of the time resolution on the light yield is presented in Fig. 18. The time resolution depends on photostatistics and is proportional to $1/\sqrt{N_{pe}}$. At a typical l.y. of 15 p.e./MIP $\sigma_t = 1.75$ ns is obtained. The time resolution of the S–counter is mainly determined by the slow decay time of the Y11 fiber. Green light travels along a WLS fiber at a speed of 17 cm/ns while the signal propagates along the counter at a smaller speed of 7.4 cm/ns because of the fiber routing. The time spectra for 3 positions of the beam along the S–counter are shown in Fig. 19. The obtained time difference between left and right signals allows us to extract the beam coordinate along

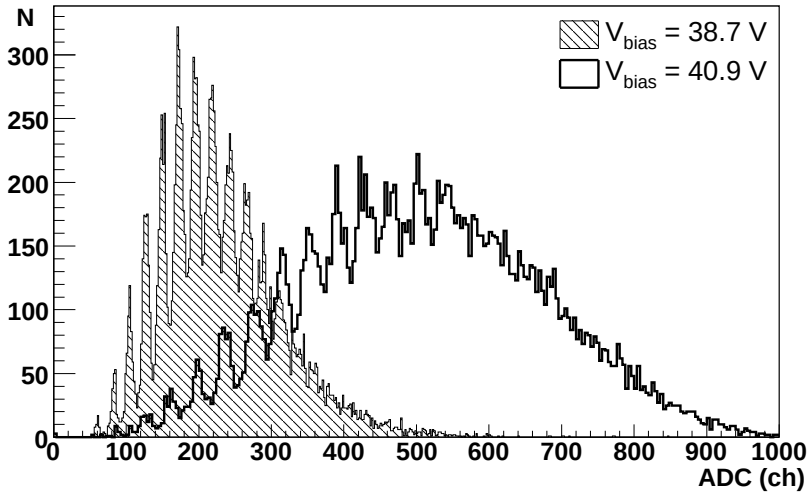

Figure 15: The spectra of 1.4 GeV/c pions measured at two bias voltages.

the S–counter using the expression

$$x(T) = 7.4[\frac{\text{cm}}{\text{ns}}] \times (T_{left} - T_{right})/2. \tag{3}$$

A spatial resolution of $\sigma_x = 13.4$ cm is obtained in the center of the S–counter and $\sigma_{x(T)} = 10.4$ cm near both ends.

The spatial resolution can be improved taking into account the light attenuation along the fiber. The asymmetry between the signals from the left and right MRS photodiodes $(A_{left} - A_{right})/(A_{left} + A_{right})$ is sensitive to the hit position of a MIP, but the spatial resolution obtained using the l.y. attenuation is poor ($\sigma_{x(A)} \sim 35$ cm) because of large fluctuations in the light yields. However, the combination of both methods

$$x = \frac{x(T) + wx(A)}{1 + w}, \tag{4}$$

where $x(T)$ and $x(A)$ are the MIP positions obtained from timing and amplitude asymmetry with accuracies of $\sigma_{x(T)}$ and $\sigma_{x(A)}$, respectively. The weight w is given by $w = \sigma^2_{x(T)}/\sigma^2_{x(A)}$, allows us to slightly improve the spatial resolution. Fig. 20 shows the spatial resolution for three beam positions obtained for the combination of the signal timing and amplitude. The spatial resolution in the center of the S–counter is obtained to be 12.4 cm, while it is about 9.9 cm at both ends.

5 Conclusion

The scintillator counters for the SMRD of the T2K near detector have been designed and tested. The readout of the extruded scintillator counters is provided via a WLS

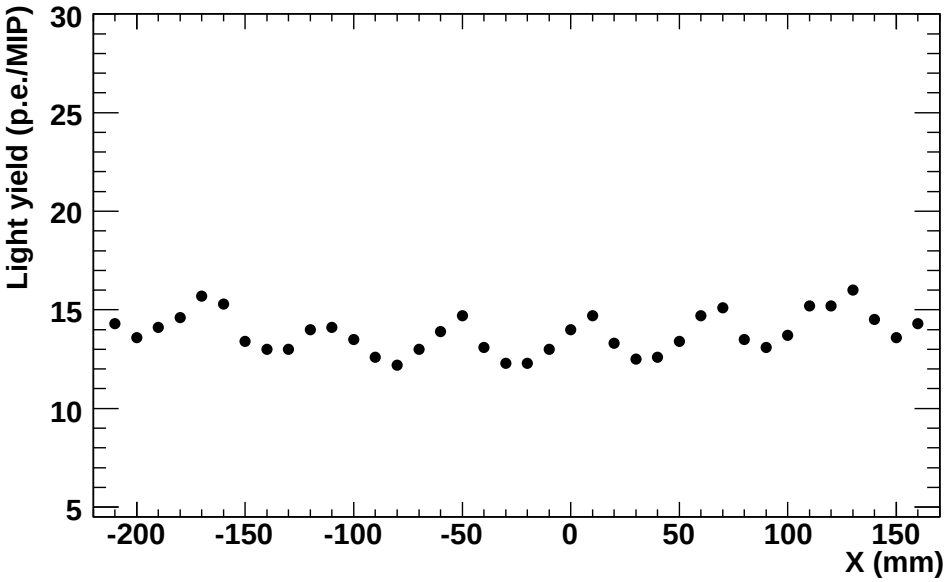

Figure 16: The light yield scan of the S–counter along the x-axis. The beam spot size is 0.5×0.5 cm^2, the scan step size is 1 cm. The sine–like waveform corresponds to the WLS fiber route with 58 mm spacing between neighboring segments.

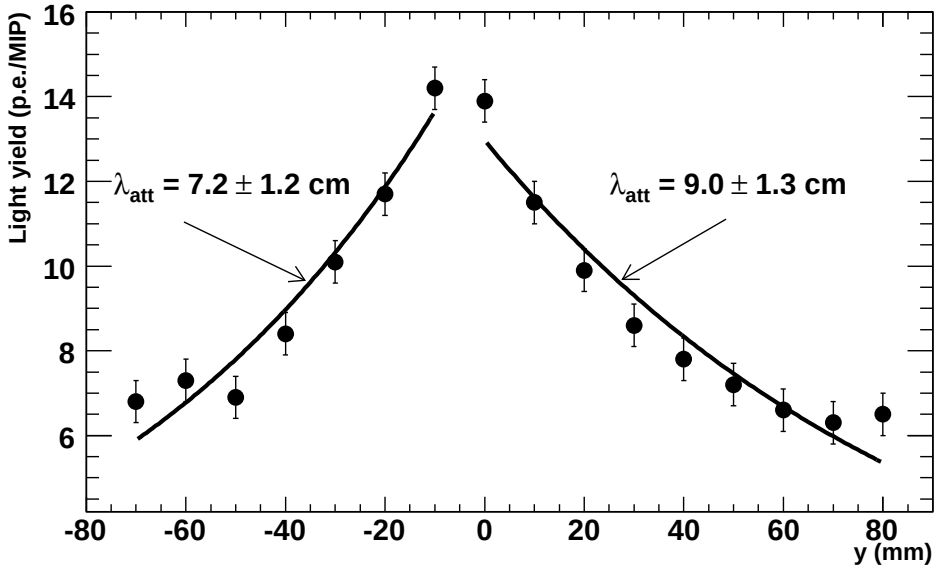

Figure 17: The light yield scan of the W-counter along the y–axis , that is perpendicular to the fiber direction. The beam spot size is 0.5×0.5 cm^2, and the scan step size is 1 cm.

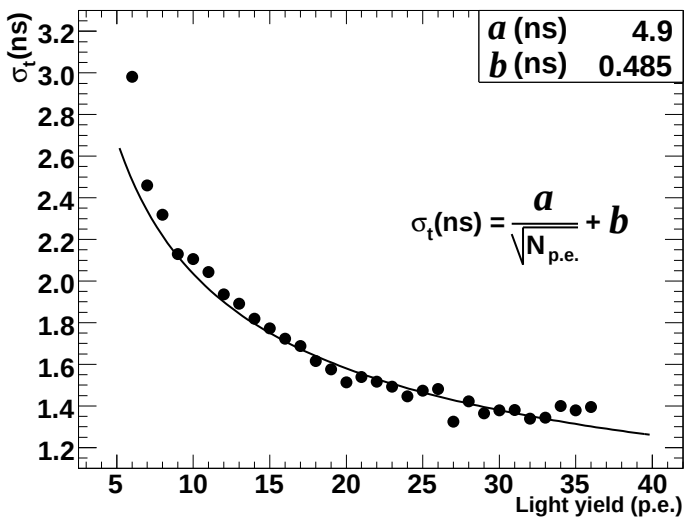

Figure 18: The time resolution versus light yield in the center of the S–counter.

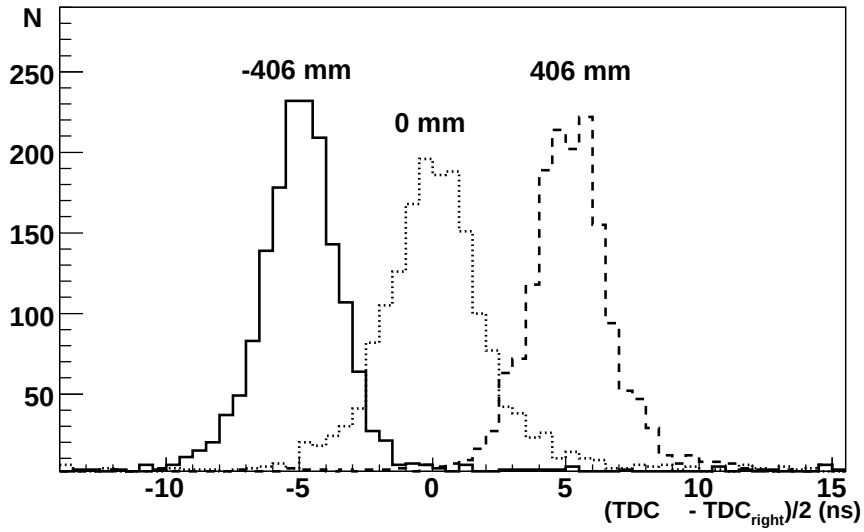

Figure 19: Time spectra for 3 positions along the S–counter. A distance of 81.2 cm corresponds to the time shift of 11 ns between the left and right MRS signals.

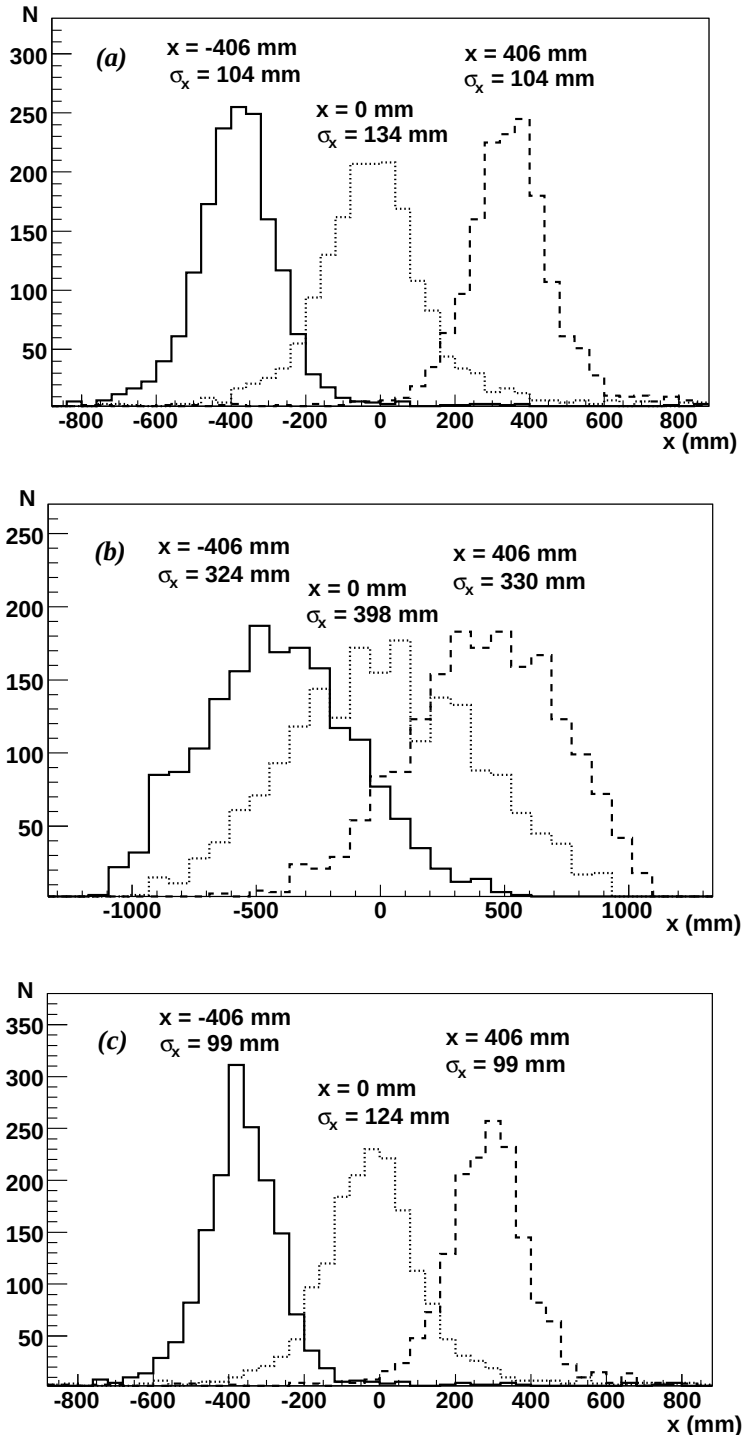

Figure 20: The spatial resolution along the S–counter at 3 beam positions: (a) the coordinate x is obtained from timing; (b) the coordinate x is obtained from the asymmetry between light yields at the two counter ends; (c) the combined position resolution.

fiber which is embedded into an S–shape groove and viewed from both ends by multi–pixel avalanche photodiodes operating in the limited Geiger mode. The studied MRS photodiodes demonstrate good performance: a low cross-talk of a few per cent, the photon detection efficiency for green light of about 12%, and a long term stability. These devices are insensitive to magnetic fields, their calibration and stability control can be provided by means of the excellent p.e. peak resolution. The linearity range of the tested MRS photodiodes is less than 200 p.e. and the recovery time is about 5 μs. Although these parameters might be critical for some applications, this performance is acceptable for many detectors of the ND280 complex of the T2K experiment.

An average l.y. of about 15 p.e./MIP, a MIP detection efficiency greater than 99.5%, a time resolution of 1.75 ns for a MIP, and a spatial resolution of $\sigma_x = 9.9 - -12.4$ cm were obtained in a pion beam test.

The authors are grateful to D. Renker, A. Akindinov and A. Konaka for useful discussions. This work was supported in part by the "Neutrino Physics" Programme of the Russian Academy of Sciences.

References

[1] Y. Itow *et al.,* hep-ex/0106019.

[2] "T2K ND280 Conceptual Design Report", T2K Internal Document.

[3] D. Drakoulakos *et al.,* hep-ex/0405002.

[4] K. Nitta *et al.,* Nucl. Instr. Meth. **A535** (2004) 147; S. Yamamoto *et al.*, IEEE Trans. Nucl. Sci. **52** (2005) 2992.

[5] E. Aliu *et al.,* K2K Collaboration, Phys. Rev. Lett. **94**, 081802 (2005); S. Yamamoto *et al.,* K2K Collaboration, Phys. Rev. Lett. **96**, 181801 (2006).

[6] G. Bondarenko, V. Golovin, M. Tarasov, Patent for invention in Russia No. 2142175, 1999.

[7] V. Golovin *et.al.,* Patent for invention in Russia, No. 1644708, 1989; A.G. Gasanov *et al.,* Lett. J. Techn. Phys. **16** (1990) 14 (in Russian).

[8] Z.Ya. Sadygov *et al.*, Nucl. Instr. Meth. **A504** (2003) 301.

[9] G. Bondarenko *et al.,* Nucl. Instr. Meth., **A442** (2000) 187.

[10] P. Buzhan *et al.*, Nucl. Instr. Meth. **A504** (2003) 48.

[11] V. Andreev *et al.,* Nucl. Instr. Meth., **A540** (2005) 368.

[12] D. Beznosko *et al.,* FERMILAB-PUB-05-410.

[13] A. Akindinov *et al.,* Nucl. Instr. Meth. **A387** (1997) 231.

[14] Kuraray Co., Ltd., Scintillator Fiber Products, 1994.

[15] E. Gushchin et al., "Multi-pixel Geiger-mode avalanche photodiodes with high quantum efficiency and low excess noise factor", Proceedings of the 4th Int. Conf. on New Developments in Photodetection, Beaune, 2005, to be published in NIM.

[16] Yu.G. Kudenko *et al.,* Nucl. Instr. Meth. **A469** (2001) 340; O. Mineev *et al.*, Nucl. Instr. Meth. **A494** (2002) 362; N. Yershov *et al.*, Nucl. Instr. Meth. **A543** (2005) 454.